Molecular Dynamics Simulation on Water/Oil Interface with Model Asphaltene Subjected to Electric Field

Wenhui Li [a], Hongbo Zeng [a, *], and Tian Tang [b, *]

[a] Department of Chemical and Materials Engineering, University of Alberta, Edmonton, AB T6G 1H9, Canada

[b] Department of Mechanical Engineering, University of Alberta, Edmonton, AB T6G 1H9, Canada

** Corresponding authors:*

E-mail: hongbo.zeng@ualberta.ca (H.Z.); Phone: +1-780-492-1044;

E-mail: tian.tang@ualberta.ca (T.T.); Phone: +1-780-492-5467.

Abstract

Hypothesis: The droplet-medium interfaces of petroleum emulsions are often stabilized by the indigenous surface-active compounds (*e.g.*, asphaltenes), causing undesired issues. While demulsification by electric field is a promising technique, fundamental study on the droplet-medium interface influenced by electric field is limited. Molecular dynamics (MD) simulations are expected to provide microscopic insights into the nano-scaled water/oil interface.

Methods: MD simulations are conducted to study the adsorption of model asphaltene molecules (represented by N-(1-hexylheptyl)-N'-(5-carboxylicpentyl) perylene-3,4,9,10-tetracarboxylic bisimide (C5Pe)) on a water-toluene interface under various strengths of electric field. The adsorption amount and structural feature of C5Pe molecules at water-toluene interface are investigated, and the effects of electric field and salt are discussed.

Findings: C5Pe molecules tend to adsorb on the water-oil interface. As the electric field strength increases, the adsorption amount first slightly increases (or remains constant) and then decreases. The electric field disrupts the compact π-π stacking between C5Pe molecules and increases their mobility, causing a dispersed distribution of the molecules with a wide range of orientations relative to the interface. Within the studied range, the addition of salt ions appears to stabilize the interface at high electric field. These results provide useful insights into the mechanism and feasibility of demulsification under electric field.

Keywords: Water/oil/model asphaltene interface; Demulsification; Electric field; Salt ions; Molecular dynamics simulation

1. Introduction

Emulsion as a type of colloids, contains a dispersed phase scattering in another immiscible continuous phase, with a boundary between them called “interface” [1-4]. Emulsions are

commonly encountered in a variety of industrial processes such as petroleum exploitation and refinement, food processing, and metal manufacturing [1-4]. Stable emulsions can be either desired or undesired based on the specific needs. For instance, milk plants add biopolymers to increase the stability of milk emulsions, preventing the formation of sugar and ice crystals [5]. However, in bitumen froth treatment in oil sands production, water-in-oil, oil-in-water, or other more complex emulsions are normally stabilized by the indigenous polar compounds in the crude oil, such as asphaltenes and resins [6-8]. These stable emulsions could cause technical challenges such as corrosion and fouling, which significantly increases the operation and production cost and leads to environmental concerns [1-4]. Therefore, it is important to investigate strategies for effective and cost-efficient demulsification.

Two categories of methods have been used to demulsify the emulsions, chemical and physical [4]. The former involves the use of chemical agents to destabilize the emulsified droplets, which, however, could be expensive and introduce secondary pollution for some operations [4, 9-11]. Physical demulsification applies external fields such as electricity, heat, ultrasound, and microwave to facilitate the coalescence and aggregation of the emulsified droplets [4, 6, 12-14]. These techniques avoid introducing expensive chemicals and show a great potential in practical applications. In particular, demulsification via electric field has drawn much interest and effort recently [4, 12, 15-18].

Existing studies on demulsification by electric field can be classified into three groups: droplet-medium interfaces [19-22], droplet electro-hydrodynamics [23-26], and droplet-droplet electro-coalescence [17, 27-30]. Since it is challenging to directly monitor the dynamic interfacial properties under an electric field, experimental studies on the droplet-medium interface are limited [18]. Mhatre et al. [22] experimentally investigated a water pendent droplet in asphaltene-

containing bulk oil (modeled by xylene), where an electric field ranging from 0 to 0.833 kV/cm was applied. It was observed that, as the electric field strength increased, the water-oil interfacial tension (IFT) decreased, while the fitted diffusion coefficient of the asphaltenes generally increased. The results were ascribed to enhanced adsorption of asphaltenes on the interface. In addition, the adsorption of asphaltene was found to be irreversible even when the electric field was turned off. Most previous studies on droplet-medium interfaces were theoretical analysis [18]. For example, Taylor et al. [31] and Lee et al. [32] predicted that the direction of flow circulation on the droplet surface under an electric field was determined by the conductivity and permittivity of the medium and droplet phase. The Sherwood number (ratio of convective and diffusive transport rates) associated with the flow circulation was found to have a positive correlation with the Peclet number (ratio of advective and diffusive transport rates) before reaching a threshold, beyond which the Sherwood number was independent of the Peclet number [19-21]. Those studies were based on continuum theories and could not provide a microscopic image of the phenomena at the interface. The molecular composition and structure in the interfacial region are also different from those in the medium and droplet phases, especially when surface-active agents are involved.

Molecular dynamics (MD) simulations are a powerful tool to complement experiments and continuum-level theories, which by their nature provides a dynamic view of atomic movements [33]. Schweighofer and Benjamin studied the water-dichloroethane interface under an electric field by MD simulations [34]. It was concluded that the electric field broadened the interfacial width by increasing the distortion of the interface. However, to our knowledge, no atomic-scale study is available on the drop-medium interface stabilized by surface-active compounds (*e.g.*, asphaltenes) when an electric field is applied. Surface-active compounds generally contain polar groups and react to the electric field [22]. Their adsorption behavior and structure pattern at the drop-medium

interface can have a significant influence on the stability of the emulsion. Furthermore, salt ions are commonly present in the aqueous phase of the emulsion, which might have an impact on the stability of the emulsion [35]. These issues are fundamentally important and practically relevant to industrial applications, especially in the petroleum industry.

In this work, MD simulations are used to study the droplet-medium interfacial properties under the influence of an electric field. A model water-oil interface is simulated where the oil phase is represented by toluene containing a model asphaltene. Salt ions are added to the water phase. An electric field is applied perpendicular to the interface, with varying strength. Thermodynamic and structural responses of model asphaltene molecules and ions are analyzed. The remainder of this work is organized as follow. In **Section 2**, we introduce the simulation systems and the details of the simulations. In **Section 3**, we present the effect of electric field strength on the interfacial adsorption of asphaltene. The influence of salt ions on the stability of the interface is also discussed. Key findings and potential implications are summarized in **Section 4**.

2. Simulation Method

2.1. Simulation Systems

Despite having an intrinsic curvature, the droplet-medium interface can be considered locally flat when investigating nanoscale phenomena near the interface. An example of the simulation systems is depicted in **Figure 1**. The left side of the simulation box is pure water or brine phase, and immediately to its right side is the oil phase containing randomly distributed model asphaltene molecules. Two graphene sheets are added to the left of water (brine) and the right of oil in order to rule out the artificial effect caused by periodic boundary conditions (PBCs) under the electric field. Otherwise, charged particles coming out of one end of the box under the

electric field will enter the other end of the box, by which the electric field will deviate from the pre-set value [36]. On the rightmost side of the simulation box is a large space of vacuum, which is used to screen the long-range interaction between the system and its images generated by PBCs. The thicknesses of water (brine), oil, and vacuum slabs are ~9 nm, ~16 nm, and 50 nm, respectively. The dimension of the system in the *x*-*y* plane is 9×9 nm^2.

Na^+ and Cl^- are added as salt ions, which are the most common ions in the brine [35, 37]. The model asphaltene molecules are represented by a polyaromatic compound N-(1-Hexylheptyl)-N-(5-carboxylicpentyl) perylene-3,4,9,10-tetracarboxylic bisimide (C5Pe) [38, 39], as shown in **Figure 1**, while the oil base is represented by toluene. Toluene is widely used to represent the oil phase in experiments and simulations [2, 3, 40, 41], and C5Pe captures key structural characteristics of asphaltenes and hence is commonly used as a model asphaltene [38, 39, 41-46]. The salt concentration in the brine phase is 3.4 wt%, which is a typical value found in petroleum emulsions [35, 37]. Four different concentrations of C5Pe (0, 30, 60 and 90 molecules) and four electric field strengths (0, 0.5, 1.0 and 1.5 V/nm) are considered. All the simulated systems are listed in **Table 1**. In the first eight sets of systems, a static and uniform electric field is applied in the positive *z*-direction, normal to the interface and pointing from the water (brine) phase towards the oil phase. The last set of systems (S3C90_R) is the same as S3C90 except that the electric field is reversed (in negative *z*-direction and pointing from oil to brine). This set is simulated and compared with S3C90 to examine the effect of electric field direction. The external electric field $\mathbf{E}$ exerts a force, $\mathbf{F}_{ef} = q\mathbf{E}$, on the charged particles in the simulation system, q being the charge of the particle. Note that the electric field in the MD simulations is 3 or 4 orders of magnitude higher than that in the experiments because the effect of a low electric field strength will be overshadowed by the molecules' thermal motion in the MD simulations [26-28, 47, 48].

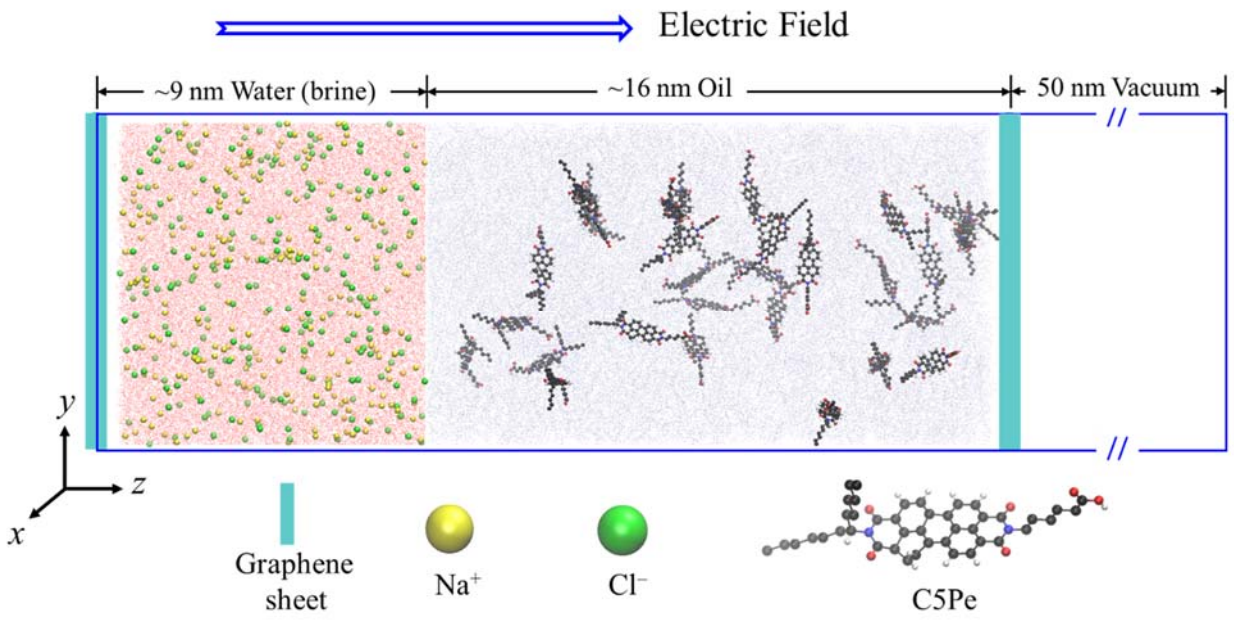

Figure 1 An example of the initial configuration of simulation systems (System S3C30 in **Table 1**). The black, red, blue, and white spheres in C5Pe molecule are C, O, N, and H respectively.

Table 1 Details of simulated systems.

System	Electric Field Strength (V/nm)	Pair of salt ions & Salt Concentration (wt%)	Number of C5Pe molecules	Number of water molecules	Number of toluene molecules
S0C0	0, 0.5, 1.0	0 & 0	0	24000	6750
S0C30	0, 0.5, 1.0	0 & 0	30	24000	6700
S0C60	0, 0.5, 1.0	0 & 0	60	24000	6650
S0C90	0, 0.5, 1.0	0 & 0	90	24000	6600
S3C0	0, 0.5, 1.0	230 & 3.4	0	23500	6750
S3C30	0, 0.5, 1.0, 1.5	230 & 3.4	30	23500	6700
S3C60	0, 0.5, 1.0, 1.5	230 & 3.4	60	23500	6650
S3C90	0, 0.5, 1.0, 1.5	230 & 3.4	90	23500	6600
S3C90_R[a]	0, 0.5, 1.0, 1.5	230 & 3.4	90	23500	6600

[a] Note: Suffix "R" represents the reversed direction of electric field.

2.2. Simulation Details

All the systems are assembled by the PACKMOL package [49] and simulations conducted using the GROMACS package (version 2021.2) [50, 51]. The energy minimization for each system is conducted by the steepest descent algorithm until the maximum force on any atom is less than 1000 kJ/(mol·nm). This step is followed by 60 ns of simulated annealing in an *NVT* ensemble, where the temperature for C5Pe is linearly raised from 300 to 500 K in the first 10 ns and then gradually quenched to 300 K in the next 50 ns. The temperature for the other components is kept at 300 K. This process helps the system to avoid being trapped in a local potential energy well. Afterward, an electric field is applied and an *NVT* equilibration is performed for at least 80 ns and up to 140 ns, with the temperature maintained at 300 K. Finally, the equilibrated system is simulated for an additional 20 ns as the sampling stage. The attainment of equilibration is confirmed by verifying that the density profiles have negligible changes in the last 20 ns of the equilibration stage and the entire sampling stage (see discussion in Section S1 of the Supporting Information (**SI**)). The graphene sheets are kept fixed during the entire simulation. Data from the last 20 ns are used for analysis.

The force field parameters are SPC for water [52], and GROMOS 54A7 [53] for the other components. The parameters of toluene and salt ions are directly from Automated Topology Builder (ATB) version 3.0 [54], while the parameterization procedure for C5Pe follows that in our previous works which have demonstrated success [2, 3, 55]. Briefly, the coordinate information of C5Pe is submitted to ATB [54] to generate the bonded and Lennard-Jones parameters, which are compatible with the GROMOS 54A7 force field. The atomic partial charges are calculated at semi-empirical level on ATB when the submitted molecule has more than 50 atoms. To improve the

accuracy, density functional theory (DFT) calculation is performed at B3LYP/6-31+G(d, p) level [56] using the Gaussian 16 package [57], and CHELPG (CHarges from ELectrostatic Potential using a Grid based method [58]) is used to determine the partial charges. These partial charges are manually mapped to the topology generated from ATB. The system setting and the force field parameters are validated by checking the induced electric field, toluene-water interfacial tension (IFT), and C5Pe behaviors in bulk solution and at the interfaces (see discussions in **SI** Section S2).

Water is rigid and bond length involving an H atom is fixed for other molecules; the constraints are achieved by the SETTLE [59] and LINCS algorithms [60], respectively. The temperature is controlled by the velocity rescaling thermostat [61] with a time constant of 0.5 ps. Three dimensional PBCs are applied. Lennard-Jones potential is truncated at 1.4 nm. While the electrostatic interaction is addressed by the three dimensional particle-mesh Ewald (PME) method [62], a force and potential correction is applied in the *z*-dimension to produce a pseudo two dimensional Ewald summation (ewald-geometry set as "3dc" in the mdp file) to further screen the long-range interaction between the system and its images in the *z*-direction. The time step is 1 fs throughout the simulation, and the trajectory is saved every 2 ps.

3. Results and Discussion

3.1. Effect of Electric Field Strength

Figure 2 presents the density (ρ) profiles of all the fluid components along the direction normal to the interface in System S3C60 under different electric fields. The density profiles in other systems are shown in SI Section S3. The *z*-axis is shifted so that the Gibbs dividing surface, where the water's surface excess is zero [63], is located at $z = 0$. The band with a lighter color around each curve represents the standard deviation from the statistical analysis of data in the last 20 ns. The densities near the graphene sheets are not analyzed or shown, to avoid the confinement

effects. In **Figure 2**, regardless of the electric field strength, C5Pe molecules show significant adsorption on the interface, demonstrated by the prominent peak near $z = 0$, while the salt ions are depleted from the interface. These are expected because C5Pe is amphiphilic, which tends to adhere to the water-oil interface [45, 46], while the salt ions (Na^+ and Cl^-) prefer to be fully hydrated by water [37, 64].

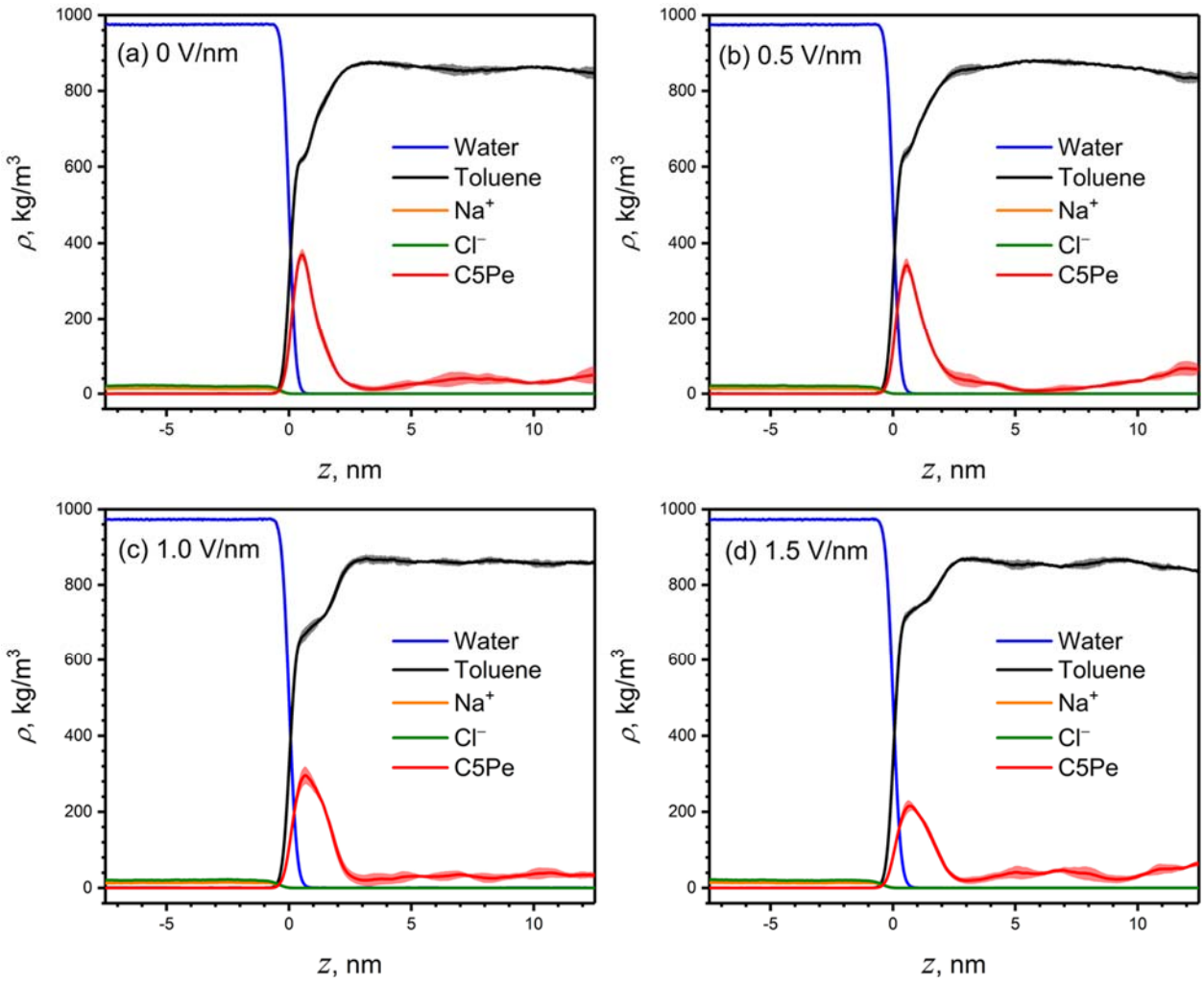

Figure 2 Density profiles of fluid components for System S3C60 along *z*-direction under various electric field strengths. The band with a lighter color around each curve represents the standard deviation.

The effect of electric field on the distribution of fluid component is further illustrated in **Figure 3** by regrouping the curves in **Figure 2**. **Figure 3(a)** shows that, as the electric field increases, the rate at which the water density decreases from its bulk value towards zero slightly decreases. **Figures 3(b)** and **(c)** suggest that, with the application of an electric field, Na^+ ions tend to approach the interface, while Cl^- ions move away from the interface. Since the applied electric field points from left to right (in the positive *z*-direction), positive ions in bulk water are driven to the right towards the interface, whereas the negative ions move in the opposite direction. **Figure 3(d)** shows an interesting trend for the distribution of C5Pe as the electric field increases: the peak value of the C5Pe density is lowered while the width of adsorbed C5Pe distribution increases. This result suggests that upon the increase in the electric field the C5Pe molecules become less concentrated near the interface and are distributed over a larger distance from the interface.

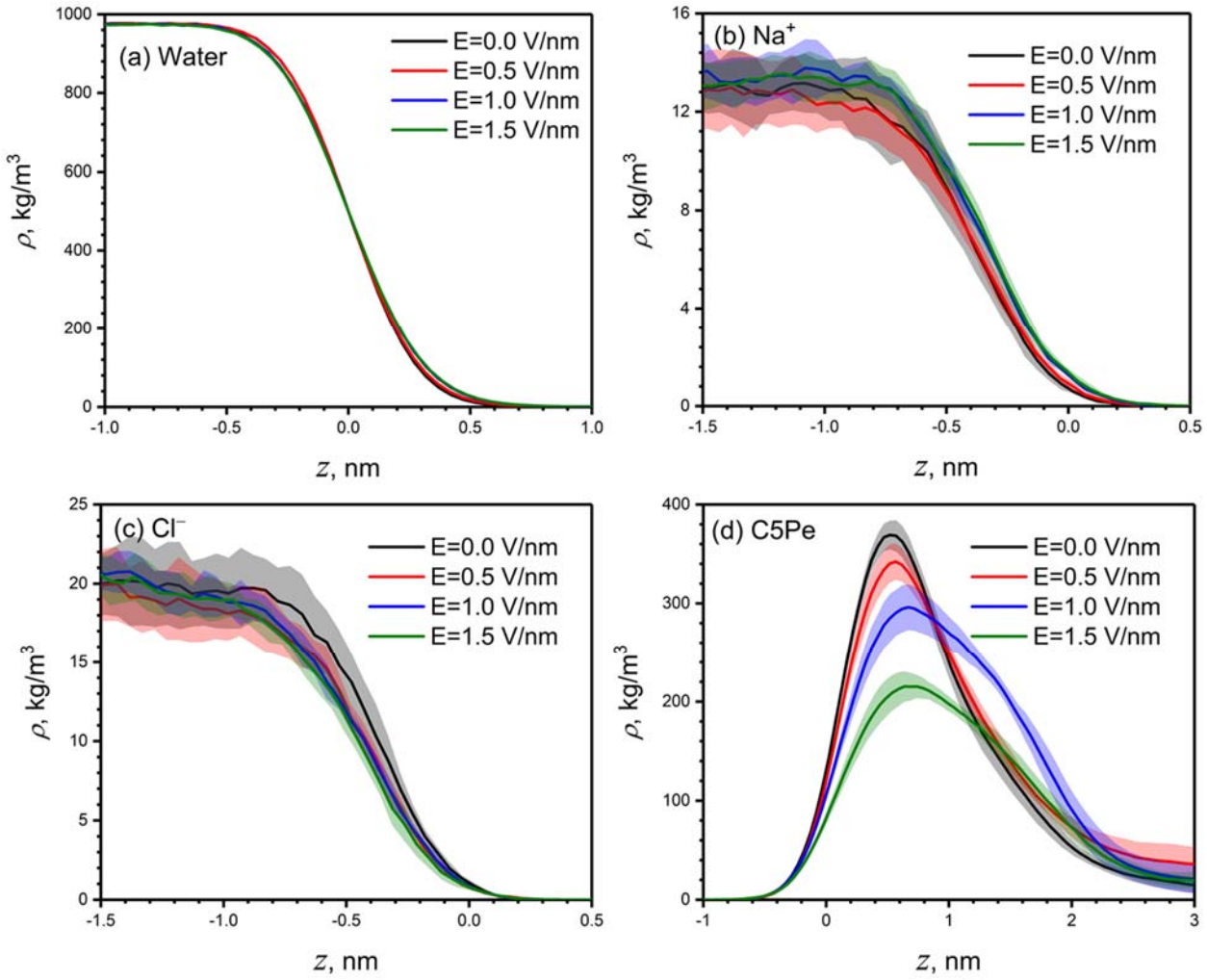

Figure 3 Comparison of the density profiles of fluid components: (a) water, (b) Na^+, (c) Cl^-, and (d) C5Pe, around the interface for System S3C60 under electric fields strength from 0 to 1.5 V/nm. The band with a lighter color around each curve represents the standard deviation.

To quantify the effect of electric field on the adsorption of C5Pe to the oil/water interface, the adsorption region is defined from z = -1 nm to z = 3 nm in **Figure 3(d)**. Beyond this range, the density of C5Pe is zero in the water phase and fluctuates around the bulk value in the toluene phase. The amount of C5Pe in the adsorption region is calculated by performing an integration of the density profile. The result of the integration is divided by the molecular mass of C5Pe to produces

the mole number of adsorbed C5Pe molecules per unit area of the interface. The final results are presented in **Figure 4(a)** as a function of the electric field, for systems with different salt and asphaltene concentrations. The adsorption amount first increases slightly (or remains constant) as the electric field increases from 0 to moderate strength (between 0.5 and 1.0 V/nm). As the electric field further increases to 1.5 V/nm, the adsorption amount decreases for the systems containing salt ions, while the interface in the systems without salt experiences an instability (to be discussed in **Section 3.3**). The mean squared displacement (MSD) of C5Pe in the *z*-direction (normal to the interface) is calculated by averaging over the C5Pe molecules that are always in the adsorption region in the last 20 ns and plotted in **Figure 4(b)** for System S3C60 (see **SI** Section S4 for the results of other systems). While the C5Pe molecules in the adsorption region have limited mobility in the *z*-direction (small MSD values), an overall increasing trend is observed as the electric field increases. It is therefore expected that under a higher electric field, the C5Pe molecules in the adsorption region can exchange more frequently with those in bulk toluene. The numbers of "trapped" (those always remain in the adsorption region in the last 20 ns) and "adsorbed" (counting all C5Pe molecules in the adsorption region and averaging the count over the last 20 ns) C5Pe molecules as well as their ratios are shown in **Figure 4(c)**. The fraction of adsorbed C5Pe molecules that are trapped generally decreases with increasing electric field, confirming their enhanced mobility and more frequent exchange with the C5Pe molecules in bulk toluene. The non-monotonic trend observed in the adsorption amount of C5Pe (**Figure 4(a)**) is because that, under moderate electric field, the widening of the distribution dominates (see for example, the blue curve in **Figure 3(d)**), and the number of C5Pe molecules diffusing from bulk toluene to the adsorption region is more than or comparable to those diffusing in the opposite direction. As the electric field continues to elevate, more C5Pe molecules diffuse from the adsorption region to the bulk toluene.

Our simulation results support an experimental hypothesis that the transport rate and adsorption amount of asphaltene are both enhanced by increasing electric field [22]. If adsorbed asphaltene molecules are to be removed from the interface via the application of an electric field, our results suggest that the electric field should be strong enough and exceed a certain threshold. Otherwise, an electric field with low strength can enhance adsorption and be adverse to the asphaltene removal. The results for the adsorption of salt ions to the interface under different electric fields are presented and discussed in **SI** Section S5.

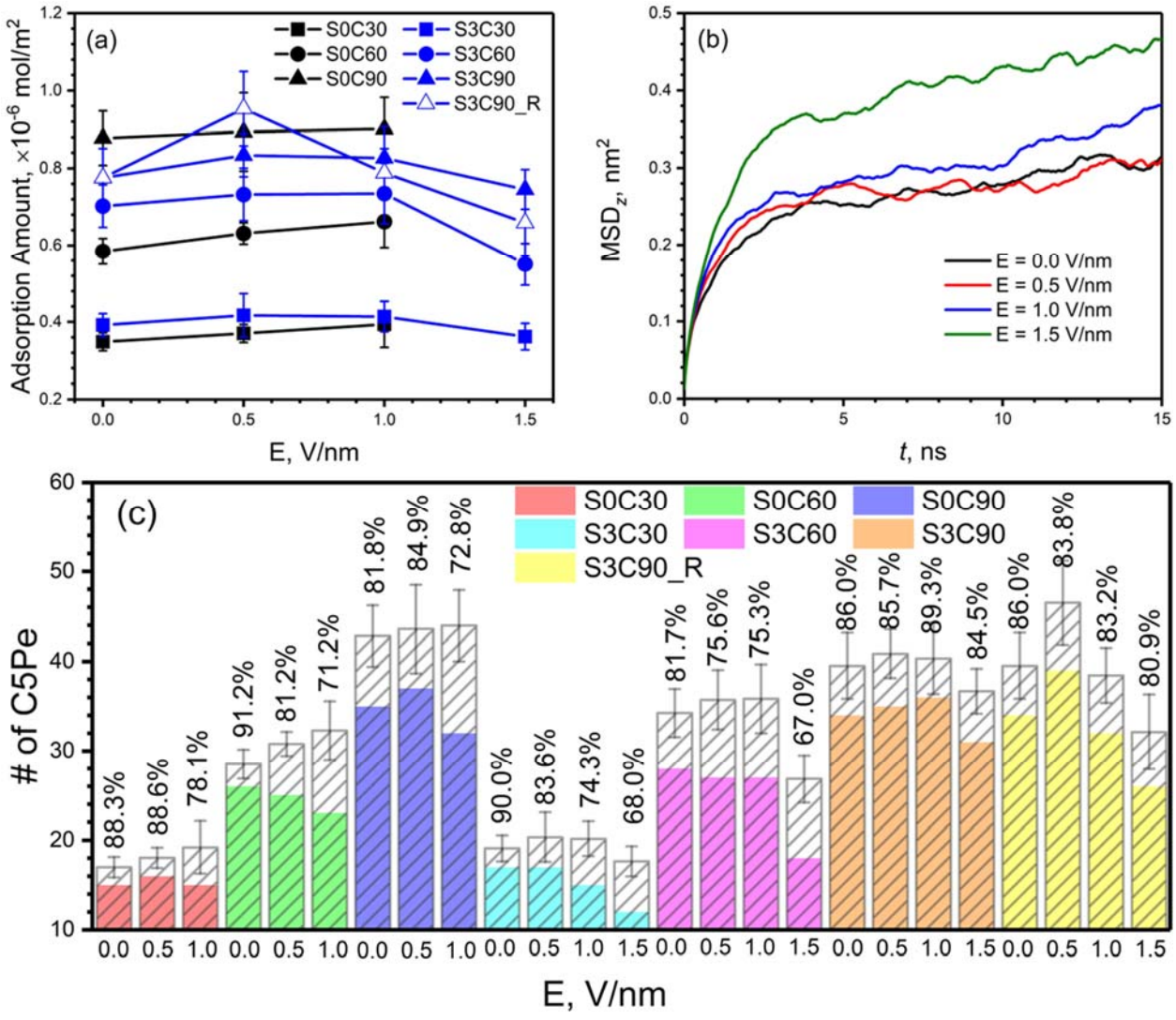

Figure 4 (a) Adsorption amount of C5Pe at water/toluene interface as a function of the electric field. (b) Mean squared displacement (MSD) of C5Pe in the *z*-direction in the adsorption region of System S3C60. (c) The number of trapped C5Pe molecules (colored columns) and the corresponding adsorbed C5Pe molecules calculated from time averaging (entire shaded columns); their ratios are labeled above the columns.

Why does the density distribution of C5Pe in the adsorption region become wider under the electric field (**Figure 3(d)**)? To explore this, the radial distribution density between the mass centers of the fused polyaromatic plane is calculated for C5Pe molecules in the adsorption region. Due to symmetry, the mass center is defined by the three carbon atoms on the center ring (see the carbon atoms enclosed by green circles in the inset of **Figure 5(a)**). **Figure 5(a)** shows the radial distribution density for System S0C30, where without applying the electric field there is a remarkable peak of ~2.36/nm^3 at the distance of ~0.47 nm. At such a short distance, the only possible structure for two C5Pe molecules is that they are aligned with their polyaromatic planes parallel to each other forming π-π stacking [35, 43]. In addition, a second peak with a much smaller value (~0.26/nm^3) can be seen at the distance of ~0.9 nm, which is about twice that of the first peak (~0.47 nm). The configuration at this distance corresponds to two C5Pe molecules separated by another C5Pe in between, forming a π-π stacked cluster. The illustration and detailed discussion of π-π interaction can be found in **SI** Section S6. **Figure 5(b)** is a snapshot of C5Pe molecules in the adsorption region of system S0C30 without electric field. This snapshot is viewed perpendicular to the interface, showing the compact distribution of C5Pe with many π-π stacks. When the electric field is applied, the first peak of the radial distribution density decreases drastically, and the second peak disappears (**Figure 5(a)**). This result indicates that the electric

field can disturb the π-π stacking between C5Pe molecules, and the cluster size is reduced. The snapshot in **Figure 5(c)** is a good illustration, which is the counterpart of **Figure 5(b)** under E = 1.0 V/nm. The C5Pe molecules are more dispersed under the electric field, with less clustering. The radial distribution densities for other systems are shown in **SI** Section S6, which in general follow the same trend as seen in **Figure 5(a)**.

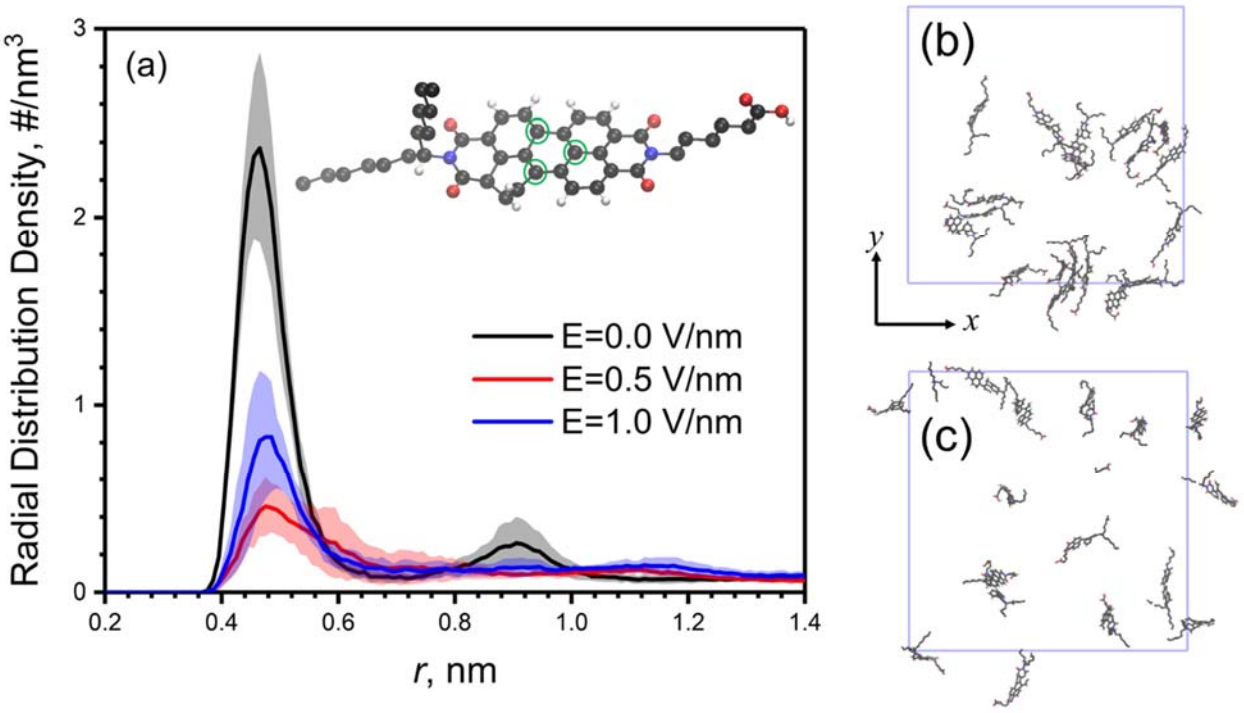

Figure 5 (a) Radial distribution density between the mass centers of the polyaromatic planes for C5Pe molecules in the adsorption region of System S0C30. Three carbon atoms enclosed by the green circles in the inset are used to define the mass center. (b) Snapshot of C5Pe in the adsorption region under E = 0 V/nm in System S0C30, viewed perpendicular to the interface. (c) Counterpart of (b) under E = 1.0 V/nm.

Combining **Figures 4** and **5**, the mechanism for the widened density distribution of C5Pe under the electric field seen in **Figure 3(d)** can be established. When the electric field is absent,

C5Pe molecules tend to aggregate and form π-π stacking, and the aggregates prefer to be perpendicular to the interface. When the electric field is introduced, π-π stacking between C5Pe molecules is weakened, and C5Pe molecules become more dispersed in the adsorption region with a wider range of orientations relative to the interface (more discussion on this in Section 3.2). As a result, C5Pe molecules are more uniformly distributed in the adsorption region. Although the total adsorption amount is increased by a moderate electric field (**Figure 4(a)**), the loosened structure in the adsorption region ((**Figure 5(c)** as compared to **Figure 5(b)**)) is beneficial for the desorption of the asphaltenes from the interface using chemical demulsifiers [3, 65].

3.2. Effect of Electric Field Direction

Systems S3C90 and S3C90_R are compared to address the effect of electric field direction. The first difference is that opposite to Systems S3C90, as the electric field strength increases, in System S3C90_R the Na^+ ions tend to retreat to the brine phase, while Cl^- ions approach the interface (see **Figures S11(f)** and **S11(g)**). This is expected because of the reversed direction of the electrostatic force acting on the ions. The second difference is the distribution of C5Pe molecules in the adsorption region. While for S3C90, as the electric field strength increases, the distribution of C5Pe becomes wider, such a trend is reversed for S3C90_R (see **Figure S11(h)**). To understand this, C5Pe orientation in the adsorption region is examined in detail and presented in **Figures 6** and **7**. For both systems, the carboxylic group (O5 and O6) is the closest to the interface, followed by O1, O2, and N1, while O3, O4, and N2 are further away from the interface. The atomic indices are shown in the insets of **Figures 6(a)** and **7(a).**

When the electric field points from brine to oil (**Figure 6**), the distances between Peak 1 (the average peak position of O5 and O6) and Peak 2 (the average peak position of O1, O2, and

N1) are 0.33 nm, 0.33 nm, 0.41 nm, and 0.41 nm, respectively, for **Figures 6(a)-(d)**. The distances in the *z*-direction between Peak 2 and Peak 3 (the average peak position of O3, O4, and N2) are 0.60 nm, 0.65 nm, 0.83 nm, and 0.85 nm, respectively, for **Figures 6(a)-(d)**. Because the locations of these peaks correspond to the most probable positions of the atom groups projected onto the *z*-axis, the gradually increasing distances between the peaks suggest that under the electric field the long axis of the C5Pe molecule is becoming more perpendicular to the interface. The orientation of the long axis can be quantified by the angle φ in **Figure 6(e)**, which is the angle between the vector connecting the two nitrogen atoms in C5Pe (vector $\boldsymbol{N_1N_2}$) and the interface (*x*-*y* plane). **Figure 6(e)** shows that in the adsorption region φ gradually increases as electric field increases. **Figure 6(f)** shows the probability distribution of the angle θ between the polyaromatic plane of C5Pe and the interface in the adsorption region. The result implies that the electric field causes the polyaromatic plane to be less perpendicular to the interface. An interesting observation can be made by combining **Figure 6(e)** and **6(f)**: when the electric field points from brine to oil, increasing the electric field causes out-of-plane rotation of the polyaromatic plane so that it becomes less perpendicular to the interface, as well as in-plane rotation rendering vector $\boldsymbol{N_1N_2}$ more perpendicular to the interface. The probability distributions of angles φ and θ for other systems are shown in **SI** Section S7, which exhibit the same characteristics.

When the electric field is reversed, pointing from oil to brine (**Figure 7**), the distances between different peaks in **Figures 7(a)-(d)** gradually decreases as electric field increases. This result is also confirmed in **Figure 7(e)**, where the vector $\boldsymbol{N_1N_2}$ becomes less perpendicular to the interface, opposite to what is observed in **Figure 6(e)**. However, similar to **Figure 6(f)**, the angle between the polyaromatic plane and the interface (θ in **Figure 7(f)**) also turns less perpendicular to the interface. Comparing **Figures 6** and **7**, reversing the direction of electric field can introduce

a different impact on the orientation of C5Pe molecules relative to the interface. Increasing electric strength in System S3C90_R causes both the polyaromatic plane and the long axis of C5Pe to be less perpendicular to the interface, which lead to narrower C5Pe distribution in the adsorption region. Despite the differences, it is interesting to see that the adsorption amount in System S3C90 follows the same non-monotonic trend in **Figure 4(a)**, which correlates well with the non-monotonic trend observed in **Figure 4(c)** for the number of C5Pe molecules trapped in the adsorption region. The potential of mean force (PMF) for a single C5Pe molecule is calculated as a function of the distance between its center of mass (COM) and the water-oil interface, under different strengths and directions of electric field. The results are shown in **SI** Section S8, which supports more favorable adsorption of C5Pe under moderate electric field strength, regardless of the direction.

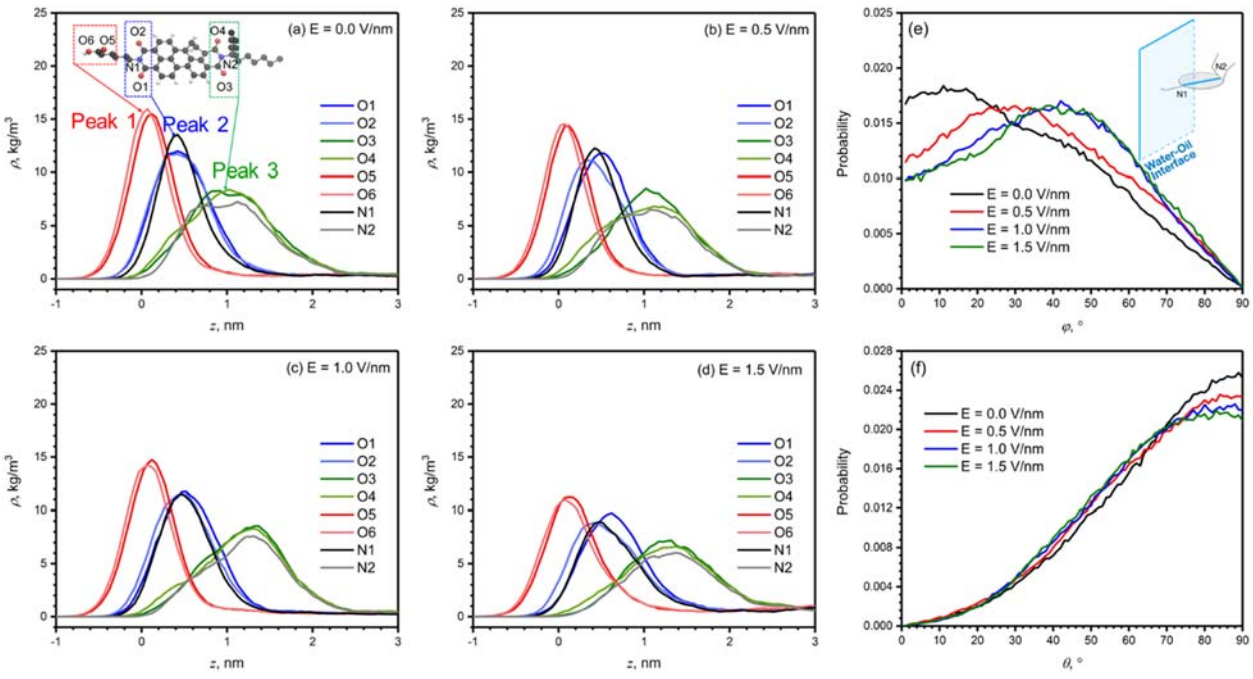

Figure 6 (a)-(d) Density of O and N atoms in C5Pe molecules along the positive z-direction in System S3C90 under various electric fields; (e) Probability distribution of the angle between the vector $\boldsymbol{N_1N_2}$ and the *x*-*y* plane, in the adsorption region of System S3C90; (f) Probability

distribution of the angle between the polyaromatic plane and the *x-y* plane, in the adsorption region of System S3C90.

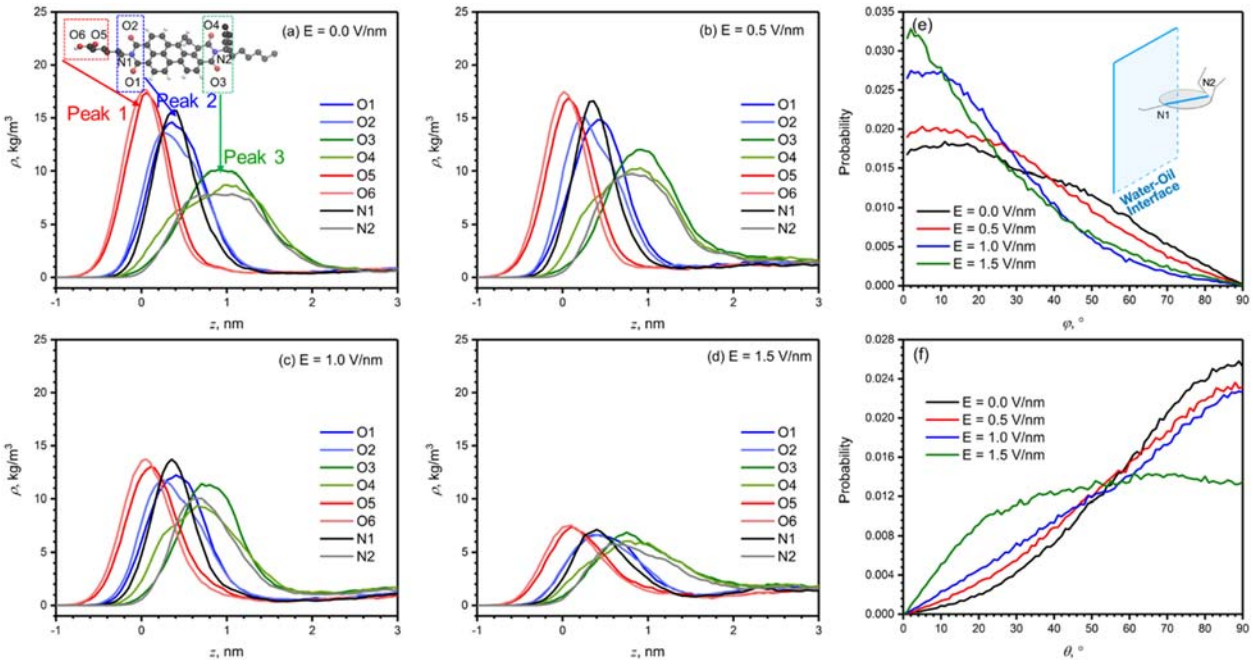

Figure 7 (a)-(d) Density of O and N atoms in C5Pe molecules along the negative z-direction in System S3C90_R under various electric fields; (e) Probability distribution of the angle between the vector $\boldsymbol{N_1N_2}$ and the *x-y* plane, in the adsorption region of System S3C90_R; (f) Probability distribution of the angle between the polyaromatic plane and the *x-y* plane, in the adsorption region of System S3C90_R.

3.3. Effects of Salt Ions and C5Pe on Interface Stability

The highest electric field that can be applied to the systems without salt or asphaltenes is 1.0 V/nm. Beyond this value, the systems become unstable with water entering the oil phase and forming a water pillar (**Figure 8**). This phenomenon was also observed by Skartlien et al. [29], and explained by considering the energy required to form a cylindrical water pillar in oil

$$U = 2\pi rL\gamma - \pi r^2\gamma - \frac{1}{2}\left(\frac{1}{k_o} - \frac{1}{k_w}\right)\varepsilon_0\pi r^2 L{E_{ext}}^2, \quad (1)$$

where γ is the IFT between water (or brine) and oil; r and L are respectively the radius and length of the cylindrical water pillar; k_w and k_o are the dielectric constants of water (or brine) and oil, respectively; ε_0 is the permittivity of vacuum; and E_{ext} is the external electric field. The first two terms on the right-hand side of Eqn. (1) are the interfacial energy required to create the additional contacting area between water (or brine) and oil, while the third term is the reduced electric energy. Sufficiently large E_{ext} can therefore make the water pillar formation an energetically favorable process.

Electric field as high as 1.5 V/nm can be applied to the systems with salt ions and C5Pe molecules, without creating any interfacial deformation. The salt ions studied in this work (Na^+ and Cl^-, at 3.4 wt%) can help stabilize the interface under high electric field. One possible reason is that the brine-oil IFT is higher than that of pure water-oil interface (see discussion in **SI** Section S9) [37, 66], which can increase the energy required to create the interfacial area between brine pillar and oil (sum of the first two terms in Eqn. (1)). Notably, this conclusion is drawn from the conditions studied in this work, and further investigations are required to examine its validity under other conditions (such as divalent ions and higher salinities). C5Pe molecules can also stabilize the interface: System S3C0 becomes unstable under the electric field of 1.5 V/nm while Systems S3C30, S3C60 and S3C90 are stable. This phenomenon is understandable because the formation of a water pillar requires the opening of a pore on the interface, which is associated with the energy-consuming reorientation of the asphaltene molecules on the interface.

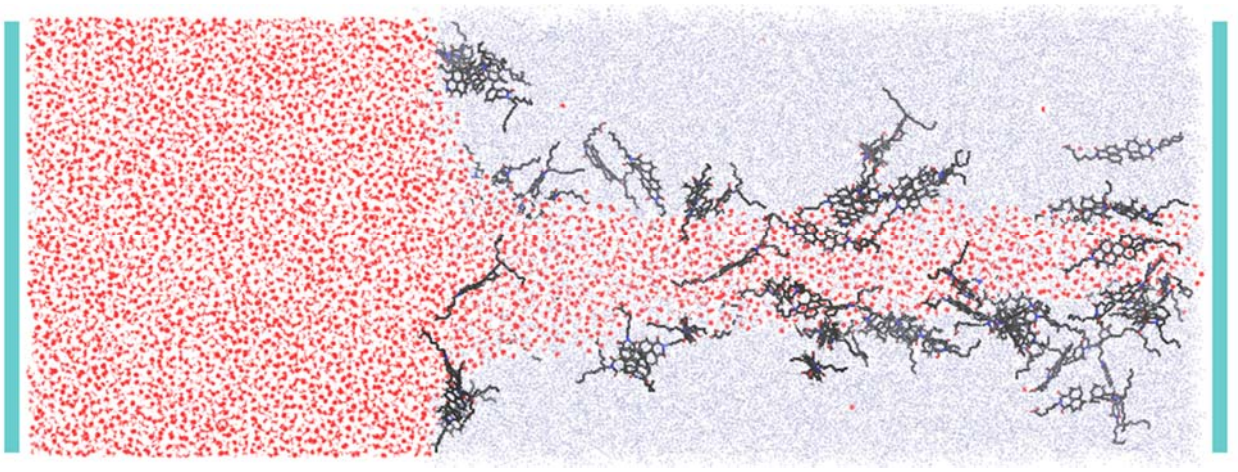

Figure 8 Example of the deformation of the water-oil interface at E = 1.5 V/nm in System S0C60. Color code same as in **Figure 1**.

4. Conclusion

In this work, MD simulations are conducted for a series of systems that mimic the droplet-medium interface during the demulsification by electric field. The thermodynamic and structural properties of water (or brine)-oil interface under the influence of an electric field were studied, where the oil phase contained various concentrations of asphaltenes modeled by C5Pe and the brine phase contained 3.4 wt% of Na^+ and Cl^-. Our results show that the C5Pe molecules tend to adsorb on the water-oil interface, and its adsorption amount first increases slightly (or remains constant) and then decreases as the strength of electric field increases. Mhatre et al. [22] also reported that the adsorption of asphaltenes increased as the electric field was increased from 0 to 0.833 kV/cm, which is in the low end of the electric field applied in the simulations and therefore in line with our finding. In the absence of electric field, C5Pe tends to aggregate and form π-π stacking, and the molecular aggregates prefer to show perpendicular configurations to the interface, which is in line with previous studies [46, 67]. The introduction of an electric field modifies the alignment of C5Pe molecules with the interface and decreases the π-π stacking between them. Consequently, C5Pe molecules become more dispersed near the interface. The electric field also

increases the mobility of C5Pe molecules and facilitates more frequent exchanges between C5Pe near the interface and those in bulk oil, which is also consistent with experimental measurement [22]. Within the range of concentrations studied in this work, the salt ions and C5Pe molecules synergistically contribute to stabilizing the interface. Under a high electric field, systems without salt ions and/or C5Pe molecules exhibit interface deformation and the formation of a water pillar into the oil phase.

To our best knowledge, this is the first atomistic-level study that investigates the behavior of asphaltene molecules at oil-water (or brine) interface under an electric field. Not only have the simulations been able to reproduce some experimental observations [22, 29, 68], they have also provided critical insights into the underlying mechanisms which are not accessible by experiments. Importantly, the newly generated understanding on the complex brine-asphaltene-oil interfacial system allows us to derive a set of guidelines for the optimization of electric field demulsification. First, the strength of the electric field should be high enough to drive the asphaltenes away from the droplet-medium interface. Otherwise, a moderate electric field can lead to increased adsorption and have an adverse effect on the asphaltene removal. Second, the simultaneous application of electric field and chemical demulsifiers is a potentially effective demulsification strategy, where the electric field breaks the asphaltene clusters into more dispersed molecules, making it easier for the chemical demulsifier (*e.g.*, non-ionic surfactant) to desorb asphaltenes from the interface [3, 65]. Finally, salt ions in the brine phase play an important role in stabilizing the droplet-medium interface, and removal or reduction of salt may facilitate the demulsification by electric fields.

Several limitations of this work and future perspectives are recognized. First, while toluene was chosen as the model oil to benefit the comparison of our work with previous studies where the same approach was used [2, 38, 41, 66, 67, 69-71], real crude oil is a complex mixture and can

influence the interfacial behaviors of asphaltenes, especially the strongly polar components [37, 72]. Accurate modeling of crude oil at molecular scale is challenging and requires more investigation. Second, the carboxylic group of C5Pe could become dissociated when the environment pH reaches or exceeds 9, which will boost its surface activity [70]. C5Pe in this work is considered charge neutral, which makes the findings applicable to environmental pH less than 9. Simulating other pH conditions is an interesting direction to pursue. Lastly, when a water droplet is subjected to an external electric field [26-28], due to surface curvature the local water-oil interfaces can experience different electric field directions (normal, parallel or slant to the interface). While in this study the electric field is only considered to be normal to the interface, work is ongoing to investigate the colloidal behavior of a water droplet immersed in the oil phase, subjected to an electric field and the presence of asphaltenes.

Acknowledgements

The authors gratefully acknowledge the computing resources and technical support from the Western Canada Research Grid (WestGrid), and the financial support from the Natural Sciences and Engineering Research Council of Canada (NSERC), Syncrude Canada Ltd., Suncor Energy, Canadian Natural Resources Limited, ChampionX, the Canada Research Chairs Program, and the Future Energy Systems under the Canada First Research Excellence Fund. The authors also thank Dr. Xiaoyu Sun for the helpful discussion and kindly providing the force field parameters of C5Pe and toluene.

References

[1] D. Wang, D. Yang, C. Huang, Y. Huang, D. Yang, H. Zhang, Q. Liu, T. Tang, M.G. El-Din, T. Kemppi, Stabilization mechanism and chemical demulsification of water-in-oil and oil-in-water emulsions in petroleum industry: A review, Fuel 286 (2021) 119390.

[2] X. Sun, D. Yang, H. Zhang, H. Zeng, T. Tang, Unraveling the Interaction of Water-in-Oil Emulsion Droplets via Molecular Simulations and Surface Force Measurements, J. Phys. Chem. B 125(27) (2021) 7556-7567.
[3] X. Sun, H. Zeng, T. Tang, Effect of non-ionic surfactants on the adsorption of polycyclic aromatic compounds at water/oil interface: A molecular simulation study, J. Colloid Interface Sci. 586 (2021) 766-777.
[4] H. Lu, Z. Pan, Z. Miao, X. Xu, S. Wu, Y. Liu, H. Wang, Q. Yang, Combination of electric field and medium coalescence for enhanced demulsification of oil-in-water emulsion, Chemical Engineering Journal Advances 6 (2021) 100103.
[5] M. BahramParvar, S.M. Razavi, Rheological interactions of selected hydrocolloid–sugar–milk–emulsifier systems, International journal of food science & technology 47(4) (2012) 854-860.
[6] S.A. Issaka, A.H. Nour, R.M. Yunus, Review on the fundamental aspects of petroleum oil emulsions and techniques of demulsification, Journal of Petroleum & Environmental Biotechnology 6(2) (2015) 1.
[7] A.A. Umar, I.B.M. Saaid, A.A. Sulaimon, R.B.M. Pilus, A review of petroleum emulsions and recent progress on water-in-crude oil emulsions stabilized by natural surfactants and solids, Journal of Petroleum Science and Engineering 165 (2018) 673-690.
[8] S.A. Raya, I.M. Saaid, A.A. Ahmed, A.A. Umar, A critical review of development and demulsification mechanisms of crude oil emulsion in the petroleum industry, Journal of Petroleum Exploration and Production Technology 10(4) (2020) 1711-1728.
[9] G. Hu, J. Li, G. Zeng, Recent development in the treatment of oily sludge from petroleum industry: a review, Journal of hazardous materials 261 (2013) 470-490.
[10] R. Zolfaghari, A. Fakhru'l-Razi, L.C. Abdullah, S.S. Elnashaie, A. Pendashteh, Demulsification techniques of water-in-oil and oil-in-water emulsions in petroleum industry, Separation and Purification Technology 170 (2016) 377-407.
[11] Z. Grenoble, S. Trabelsi, Mechanisms, performance optimization and new developments in demulsification processes for oil and gas applications, Advances in colloid and interface science 260 (2018) 32-45.
[12] T. Ichikawa, Electrical demulsification of oil-in-water emulsion, Colloids and Surfaces A: Physicochemical and Engineering Aspects 302(1-3) (2007) 581-586.

[13] R. Martínez-Palou, R. Cerón-Camacho, B. Chávez, A.A. Vallejo, D. Villanueva-Negrete, J. Castellanos, J. Karamath, J. Reyes, J. Aburto, Demulsification of heavy crude oil-in-water emulsions: A comparative study between microwave and thermal heating, Fuel 113 (2013) 407-414.
[14] X. Xu, D. Cao, J. Liu, J. Gao, X. Wang, Research on ultrasound-assisted demulsification/dehydration for crude oil, Ultrasonics sonochemistry 57 (2019) 185-192.
[15] E. Mohammadian, T.S. Taju Ariffin, A. Azdarpour, H. Hamidi, S. Yusof, M. Sabet, E. Yahya, Demulsification of light malaysian crude oil emulsions using an electric field method, Industrial & Engineering Chemistry Research 57(39) (2018) 13247-13256.
[16] B. Ren, Y. Kang, Demulsification of oil-in-water (O/W) emulsion in bidirectional pulsed electric field, Langmuir 34(30) (2018) 8923-8931.
[17] S. Mhatre, T. Hjartnes, S. Simon, J. Sjöblom, Coalescence behavior of stable pendent drop pairs held at different electric potentials, Langmuir 36(7) (2020) 1642-1650.
[18] J. Sjöblom, S. Mhatre, S. Simon, R. Skartlien, G. Sørland, Emulsions in external electric fields, Advances in Colloid and Interface Science (2021) 102455.
[19] F. Morrison Jr, Transient heat and mass transfer to a drop in an electric field, (1977).
[20] D.L. Oliver, T.E. Carleson, J.N. Chung, Transient heat transfer to a fluid sphere suspended in an electric field, International journal of heat and mass transfer 28(5) (1985) 1005-1009.
[21] D. Oliver, K. De Witt, High Peclet number heat transfer from a droplet suspended in an electric field: interior problem, International journal of heat and mass transfer 36(12) (1993) 3153-3155.
[22] S. Mhatre, S. Simon, J. Sjoblom, Experimental Evidence of Enhanced Adsorption Dynamics at Liquid–Liquid Interfaces under an Electric Field, Analytical Chemistry 92(19) (2020) 12860-12870.
[23] S.D. Deshmukh, R.M. Thaokar, Deformation, breakup and motion of a perfect dielectric drop in a quadrupole electric field, Physics of Fluids 24(3) (2012) 032105.
[24] S. Mhatre, R.M. Thaokar, Drop motion, deformation, and cyclic motion in a non-uniform electric field in the viscous limit, Physics of Fluids 25(7) (2013) 072105.
[25] D. Yang, Y. Sun, M. Ghadiri, H. Wu, H. Qiao, L. He, X. Luo, Y. Lü, Effect of hydrolyzed polyacrylamide used in polymer flooding on droplet–interface electro-coalescence: Variation of

critical electric field strength of partial coalescence, Separation and Purification Technology 227 (2019) 115737.
[26] N. Li, Z. Sun, W. Liu, L. Wei, B. Li, Z. Qi, Z. Wang, Effect of electric field strength on deformation and breakup behaviors of droplet in oil phase: A molecular dynamics study, J. Mol. Liq. 333 (2021) 115995.
[27] B.-B. Wang, X.-D. Wang, W.-M. Yan, T.-H. Wang, Molecular dynamics simulations on coalescence and non-coalescence of conducting droplets, Langmuir 31(27) (2015) 7457-7462.
[28] B.-B. Wang, X.-D. Wang, T.-H. Wang, G. Lu, W.-M. Yan, Electro-coalescence of two charged droplets under constant and pulsed DC electric fields, Int. J. Heat Mass Transfer 98 (2016) 10-16.
[29] R. Skartlien, S. Simon, J. Sjöblom, Electrocoalescence of water in oil emulsions: a DPD simulation study and a novel application of electroporation theory, RSC advances 9(59) (2019) 34172-34183.
[30] B. Li, Z. Wang, V. Vivacqua, M. Ghadiri, J. Wang, W. Zhang, D. Wang, H. Liu, Z. Sun, Z. Wang, Drop-interface electrocoalescence mode transition under a direct current electric field, Chem. Eng. Sci. 213 (2020) 115360.
[31] G.I. Taylor, Studies in electrohydrodynamics. I. The circulation produced in a drop by an electric field, Proceedings of the Royal Society of London. Series A. Mathematical and Physical Sciences 291(1425) (1966) 159-166.
[32] S. Lee, D. Im, I. Kang, Circulating flows inside a drop under time-periodic nonuniform electric fields, Physics of Fluids 12(8) (2000) 1899-1910.
[33] D. Frenkel, B. Smit, Understanding molecular simulation: from algorithms to applications, Elsevier2001.
[34] K.J. Schweighofer, I. Benjamin, Electric field effects on the structure and dynamics at a liquid| liquid interface, Journal of Electroanalytical Chemistry 391(1-2) (1995) 1-10.
[35] X. Sun, C. Jian, Y. He, H. Zeng, T. Tang, Probing the Effect of Salt on Asphaltene Aggregation in Aqueous Solutions Using Molecular Dynamics Simulations, Energy Fuels 32(8) (2018) 8090-8097.
[36] C. Caleman, D. Van Der Spoel, Picosecond melting of ice by an infrared laser pulse: A simulation study, Angewandte Chemie International Edition 47(8) (2008) 1417-1420.

[37] W. Li, Y. Nan, X. Wen, W. Wang, Z. Jin, Effects of Salinity and N-, S-, and O-Bearing Polar Components on Light Oil–Brine Interfacial Properties from Molecular Perspectives, J. Phys. Chem. C 123(38) (2019) 23520-23528.
[38] J. Wang, N. van der Tuuk Opedal, Q. Lu, Z. Xu, H. Zeng, J. Sjoblom, Probing molecular interactions of an asphaltene model compound in organic solvents using a surface forces apparatus (SFA), Energy Fuels 26(5) (2012) 2591-2599.
[39] J. Wang, Q. Lu, D. Harbottle, J. Sjoblom, Z. Xu, H. Zeng, Molecular interactions of a polyaromatic surfactant C5Pe in aqueous solutions studied by a surface forces apparatus, J. Phys. Chem. B 116(36) (2012) 11187-11196.
[40] F. Yang, P. Tchoukov, P. Qiao, X. Ma, E. Pensini, T. Dabros, J. Czarnecki, Z. Xu, Studying demulsification mechanisms of water-in-crude oil emulsions using a modified thin liquid film technique, Colloids and Surfaces A: Physicochemical and Engineering Aspects 540 (2018) 215-223.
[41] Y. Xiong, T. Cao, Q. Chen, Z. Li, Y. Yang, S. Xu, S. Yuan, J. Sjoblom, Z. Xu, Adsorption of a polyaromatic compound on silica surfaces from organic solvents studied by molecular dynamics simulation and AFM imaging, J. Phys. Chem. C 121(9) (2017) 5020-5028.
[42] J. Sjöblom, S. Simon, Z. Xu, Model molecules mimicking asphaltenes, Advances in colloid and interface science 218 (2015) 1-16.
[43] R.B. Teklebrhan, L. Ge, S. Bhattacharjee, Z. Xu, J. Sjöblom, Probing structure–nanoaggregation relations of polyaromatic surfactants: a molecular dynamics simulation and dynamic light scattering study, J. Phys. Chem. B 116(20) (2012) 5907-5918.
[44] R.B. Teklebrhan, C. Jian, P. Choi, Z. Xu, J. Sjöblom, Role of naphthenic acids in controlling self-aggregation of a polyaromatic compound in toluene, The Journal of Physical Chemistry B 120(14) (2016) 3516-3526.
[45] F. Gao, Z. Xu, G. Liu, S. Yuan, Molecular dynamics simulation: the behavior of asphaltene in crude oil and at the oil/water interface, Energy Fuels 28(12) (2014) 7368-7376.
[46] G. Lv, F. Gao, G. Liu, S. Yuan, The properties of asphaltene at the oil-water interface: A molecular dynamics simulation, Colloids and Surfaces A: Physicochemical and Engineering Aspects 515 (2017) 34-40.
[47] Y. Zhao, K. Dong, X. Liu, S. Zhang, J. Zhu, J. Wang, Structure of ionic liquids under external electric field: a molecular dynamics simulation, Molecular Simulation 38(3) (2012) 172-178.

[48] M.T. Nguyen, Q. Shao, Effect of Zwitterionic Molecules on Ionic Transport under Electric Fields: A Molecular Simulation Study, Journal of Chemical & Engineering Data 65(2) (2019) 385-395.
[49] L. Martínez, R. Andrade, E.G. Birgin, J.M. Martínez, PACKMOL: a package for building initial configurations for molecular dynamics simulations, J. Comput. Chem. 30(13) (2009) 2157-2164.
[50] H.J. Berendsen, D. van der Spoel, R. van Drunen, GROMACS: a message-passing parallel molecular dynamics implementation, Comput. Phys. Commun. 91(1-3) (1995) 43-56.
[51] D. Van Der Spoel, E. Lindahl, B. Hess, G. Groenhof, A.E. Mark, H.J. Berendsen, GROMACS: fast, flexible, and free, J. Comput. Chem. 26(16) (2005) 1701-1718.
[52] H.J. Berendsen, J.P. Postma, W.F. van Gunsteren, J. Hermans, Interaction models for water in relation to protein hydration, Intermolecular forces, Springer1981, pp. 331-342.
[53] N. Schmid, A.P. Eichenberger, A. Choutko, S. Riniker, M. Winger, A.E. Mark, W.F. van Gunsteren, Definition and testing of the GROMOS force-field versions 54A7 and 54B7, European biophysics journal 40(7) (2011) 843-856.
[54] M. Stroet, B. Caron, K.M. Visscher, D.P. Geerke, A.K. Malde, A.E. Mark, Automated topology builder version 3.0: Prediction of solvation free enthalpies in water and hexane, Journal of chemical theory and computation 14(11) (2018) 5834-5845.
[55] X. Sun, H. Zeng, T. Tang, Molecular simulation of folding and aggregation of multi-core polycyclic aromatic compounds, J. Mol. Liq. 310 (2020) 113248.
[56] A.D. Becke, A new mixing of Hartree‐Fock and local density‐functional theories, J. Chem. Phys. 98(2) (1993) 1372-1377.
[57] M. Frisch, G. Trucks, H. Schlegel, G. Scuseria, M. Robb, J. Cheeseman, G. Scalmani, V. Barone, G. Petersson, H. Nakatsuji, Gaussian 16 Revision C. 01, 2016, Gaussian Inc. Wallingford CT 1 (2016).
[58] C.M. Breneman, K.B. Wiberg, Determining atom‐centered monopoles from molecular electrostatic potentials. The need for high sampling density in formamide conformational analysis, J. Comput. Chem. 11(3) (1990) 361-373.
[59] S. Miyamoto, P.A. Kollman, Settle: An analytical version of the SHAKE and RATTLE algorithm for rigid water models, J. Comput. Chem. 13(8) (1992) 952-962.

[60] B. Hess, P-LINCS: A parallel linear constraint solver for molecular simulation, Journal of chemical theory and computation 4(1) (2008) 116-122.
[61] G. Bussi, D. Donadio, M. Parrinello, Canonical sampling through velocity rescaling, J. Chem. Phys. 126(1) (2007) 014101.
[62] U. Essmann, L. Perera, M.L. Berkowitz, T. Darden, H. Lee, L.G. Pedersen, A smooth particle mesh Ewald method, J. Chem. Phys. 103(19) (1995) 8577-8593.
[63] D. Chattoraj, Adsorption and the Gibbs surface excess, Springer Science & Business Media2012.
[64] W. Li, Z. Jin, Effect of ion concentration and multivalence on methane-brine interfacial tension and phenomena from molecular perspectives, Fuel 254 (2019) 115657.
[65] N. Anton, T.F. Vandamme, P. Bouriat, Dilatational rheology of a gel point network formed by nonionic soluble surfactants at the oil–water interface, Soft Matter 9(4) (2013) 1310-1318.
[66] C. Jian, M.R. Poopari, Q. Liu, N. Zerpa, H. Zeng, T. Tang, Mechanistic understanding of the effect of temperature and salinity on the water/toluene interfacial tension, Energy Fuels 30(12) (2016) 10228-10235.
[67] T. Kuznicki, J.H. Masliyah, S. Bhattacharjee, Aggregation and partitioning of model asphaltenes at toluene− water interfaces: Molecular dynamics simulations, Energy Fuels 23(10) (2009) 5027-5035.
[68] L. Klinger, L. Levin, Interface instability in an electric field, J. Appl. Phys. 78(3) (1995) 1669-1672.
[69] C. Jian, M.R. Poopari, Q. Liu, N. Zerpa, H. Zeng, T. Tang, Reduction of water/oil interfacial tension by model asphaltenes: the governing role of surface concentration, J. Phys. Chem. B 120(25) (2016) 5646-5654.
[70] E.L.k. Nordgård, J. Sjöblom, Model compounds for asphaltenes and C80 isoprenoid tetraacids. Part I: synthesis and interfacial activities, J. Dispersion Sci. Technol. 29(8) (2008) 1114-1122.
[71] T. Kuznicki, J.H. Masliyah, S. Bhattacharjee, Molecular dynamics study of model molecules resembling asphaltene-like structures in aqueous organic solvent systems, Energy Fuels 22(4) (2008) 2379-2389.
[72] M. Sedghi, M. Piri, L. Goual, Atomistic molecular dynamics simulations of crude oil/brine displacement in calcite mesopores, Langmuir 32(14) (2016) 3375-3384.